CSI Acquisition for Aerial IRS Supported Cell-Free Communication Systems

Sarah Tanzina¹, Imtiaz Ahmed², Md Sahabul Alam³, Lutfa Akter¹, Kamrul Hasan⁴, and Samia Tasnim⁵

¹Bangladesh University of Engineering and Technology, Dhaka, Bangladesh
 ²Howard University, Washington DC, USA, ³California State University, Northridge, CA, USA
 ⁴Tennessee State University, Nashville, TN, USA, ⁵University of Toledo, OH, USA

Abstract—In this paper, we consider a cell-free massive multiple input multiple output (CF-MMIMO) communication system, where users are supported by access points (AP) in conjunction with intelligent reflecting surfaces (IRS) mounted on unmanned aerial vehicles (UAVs). Although aerial IRS (aIRS) offers agile support for expanding network coverage in CF communication systems, the effective operation of such a complex network necessitates a channel state information (CSI) acquisition scheme that exhibits low run-time computational complexity. We propose an artificial intelligence (AI)-based approach to design and develop an efficient channel prediction scheme for CSI acquisition in the CF-MMIMO network supported by aIRS considered. Simulation results demonstrate the effectiveness of the proposed scheme in predicting channel gains across a wide range of signal-to-noise ratios (SNR) while maintaining low computational complexity during real-time operations.

Index Terms—Cell-free massive MIMO (CF-MIMO), Intelligent Reflecting Surface (IRS), Unmanned Aerial Vehicle (UAV), Deep Learning Neural Network (DNN), Channel State Information (CSI), Channel Mapping

I. INTRODUCTION

TEXT-generation wireless communication systems, such as beyond fifth generation (B5G) / sixth generation (6G) cellular communication systems, are expected to significantly increase network capacity over current fifth generation (5G) new radio (NR) systems to satisfy the ever-growing demands for higher data rates, increased energy efficiency, larger coverage area, and versatile multimodal services. For this, cellfree MMIMO (CF-MMIMO) is a potential technology that divides the conventional MMIMO base station (BS) into a large number of individually controllable antennas that act as access points (AP) in the same time/frequency band [1], [2]. This provides uniformly better quality of service (QoS) in a much larger geographical region. The intelligent reflecting surface (IRS)-supported CF-MMIMO network offers numerous constructive reflected paths for the signals transmitted from the APs [3]. The phase shifts of the IRS passive reflecting elements (PRE) are smartly tuned to increase the desired signal in the intended direction and suppress co-channel interference [4]. Furthermore, in a CF-MMIMO system, an IRS can replace some APs to improve capacity while maintaining cost and energy efficiency [5].

The communication scenario in this work (as illustrated in Fig. 1) shows that the transmitters and the receiver nodes are separated by large obstacles (e.g., towering buildings, mountains, etc.). As a result, line-of-sight (LoS) communication between them is impossible. An IRS-integrated network can establish this LoS communication path. However, the terres-

trial IRS deployment strategy is critical. To address dynamic and complex communication challenges; it is important to evaluate key variables such as network coverage, reconfigurable channel state, and passive beamforming performance [6]. The integration of IRS with UAVs, by mounting IRS panels on it, known as aerial IRS (aIRS), can be an appealing option for our system model [7], [8]. The fully controllable mobility of the UAV in the 3D space ensures the flexible deployment of aIRS in an appropriate location for favorable communication between the transmitter and receiver nodes [9]. Due to user mobility, constant repositioning of the UAV is typically required; however, adjusting IRS phase shifts can alleviate this B5G requirement [10].

In this study, we consider an aIRS-integrated CF-MMIMO communication system, where APs serve ground user equipment (UEs) with the help of aIRS panels, to enhance the performance of conventional point-to-point communications. In such a system, reliable data transmission over aIRS requires the estimation of a significant number of channel coefficients, despite the absence of active radio frequency (RF) chains. In addition, the end-to-end cascaded channels (AP-IRS-UE) are estimated instead of estimating separate channels for AP-IRS and IRS-UE, which yields high computational complexity. A least squares (LS) channel estimator for an IRS-aided singleuser CF-MMIMO system is proposed in [11]. Estimation of the direction-of-arrival (DoA)-based channel, considering that some of the IRS elements are active and have an RF chain behind them, is proposed in [12]. Furthermore, [13] considers IRS on/off element patterns for channel estimation.

Data-driven CSI acquisition schemes have shown superior performance while reducing computational complexity during runtime. Deep learning-based algorithms techniques are used to estimate downlink CSI from known uplink CSI [14], [15], [16], [17]. In our paper both uplink and downlink CSIs are unknown and the IRS is considered fully passive. The IRS-carrying UAV has active antennas with RF chains. So, considering AP-UAV and UAV-UE links known, in this paper we derived an algorithm to estimate the channels of individual AP-IRS and IRS-UE links. In particular, we decipher the underlying correlations among CSIs of different links that are co-located in space. The following two scenarios are studied for channel acquisitions in the considered aIRS-assisted CF network:

 Scenario 1: In this scenario, the channels for the AP-IRS link are predicted from the estimated channels of the AP-UAV link for a given AP.

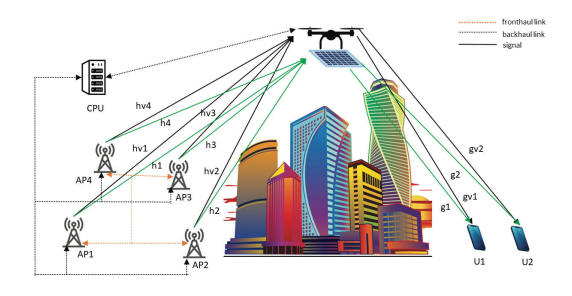


Fig. 1. System Model.

 Scenario 2: In this scenario, the channels for a set of AP-IRS links are predicted from another set of known channels of AP-IRS links estimated in Scenario 1.

Scenario 1 is the objective of this work. Scenario 2 further reduces the complexity of the CF-MMIMO system by estimating multiple AP-IRS links from one link. For each of the scenarios considered, we develop a deep neural network (DNN)-assisted channel mapping scheme that is trained offline using large training datasets. Once trained, the inference models are deployed for online channel predictions. We evaluate the performance of the proposed scheme with the baseline scheme to show its effectiveness.

II. SYSTEM AND CHANNEL MODEL

In this section, we introduce the system and channel model for the considered CF-MMIMO network.

A. System Model

Let us consider a CF-MMIMO system that is aided by an IRS-mounted UAV node, as shown in Fig. 1. The considered system has K APs that provide signal coverage to U ground (terrestrial) users. Each of the APs and users is equipped with a single antenna for data transmission. All APs are connected to the central processing unit (CPU) via high-capacity fronthaul links. The CPU is capable of high-performance computing and centralized baseband signal processing operations to support all users. An aIRS is deployed to support APs to provide coverage to users with N discrete, individually controllable reconfigurable PREs, oriented as a uniform planar array (UPA) with dimensions of N_h columns and N_v rows. We consider the IRS panel to be positioned on the X-Y plane of a Cartesian coordinate system. The UAV mounting the aIRS is equipped with L active antennas that communicate with the participating APs in the considered CF network. Unlike the PREs of the IRS panel, the UAV itself is capable of active data transmission and, therefore, estimating channels with the aid of active digital and analog chains configured with L antennas. All APs, users, and UAVs are considered fixed in their respective positions (at a given time), randomly distributed in a geographical area of $D \times D$ m², and placed at a given altitude.

B. Channel Model

In the considered system, each AP, each user, the IRS and the UAV are represented by $P_s=(x_s,y_s,z_s),\ P_d=(x_d,y_d,z_d),\ P_r=(x_r,y_r,z_r),$ and $P_u=(x_u,y_u,z_u),$ respectively, in 3D coordinates, where $P_i\in\mathbb{N}^{1\times 3}$ for $i\in\{s,d,r,u\}.$

We define $\boldsymbol{h} \in \mathbb{C}^{N \times 1}$ as the channel from AP to IRS, $\boldsymbol{h}_v \in \mathbb{C}^{L \times 1}$ as the channel from AP to UAV, $\boldsymbol{g} \in \mathbb{C}^{1 \times N}$ as the channel from IRS to user and $\boldsymbol{g}_v \in \mathbb{C}^{1 \times L}$ as the channel from UAV to user. All these channels are considered to be time-varying Rician fading, consisting of both LoS and non-LoS (NLoS) components. Therefore, the LoS component of \boldsymbol{h} , denoted as \boldsymbol{h}_{LoS} , is modeled as [18].

$$\boldsymbol{h}_{LoS} = \sqrt{\frac{\Gamma_h K_h}{1 + K_h}} \exp\left(j2\pi n \frac{f}{f_s}\right) \boldsymbol{a}_h(\theta_h, \phi_h),$$
 (1)

where Γ_h = $10^{\frac{PL_0}{10}-\gamma log\frac{d_h}{d_0}}$ represents the transmission path loss between the AP and the IRS. Here, γ and K_h are the path loss exponent and the Rician K factor, respectively. PL_0 represents the path loss at the reference distance of $d_0=1$ m. Moreover, the distance between an AP and the IRS is defined as d_h , which can be calculated as

$$d_h = \sqrt{(x_s - x_r)^2 + (y_s - y_r)^2 + (z_s - z_r)^2}.$$
 (2)

The array response vector of the IRS panel is given by [18]

$$\boldsymbol{a}_h(\theta_h, \phi_h) = [1, \dots, \exp(j\frac{2\pi}{\lambda}d)$$

$$((N_h - 1)\sin\theta_h\cos\phi_h + (N_v - 1)\sin\phi_h)]^T, \quad (3)$$

where the azimuth angle of arrival (AoA) and the elevation AoA are denoted as $\theta_h = \arccos\frac{z_s-z_r}{d_h}$ and $\phi_h = \arctan\frac{y_s-y_r}{x_s-x_r}$, respectively. Furthermore, the wavelength is denoted as $\lambda = c/f$, and the spacing between two consecutive PREs of IRS is represented as $\Delta = \lambda/2$. Here, f is the carrier frequency and f_s is the system bandwidth. On the other hand, the antennas of UAV are modeled as a uniform linear array (ULA), and its array response vector is given by

$$\boldsymbol{a}_{hv}(\theta_{hv}, \phi_{hv}) = [1, \dots, \exp(j\frac{2\pi}{\lambda}d)(L-1)\sin\theta_{hv}\cos\phi_{hv}]^T.$$
(4)

Each element of the non-LoS component of h, denoted as h_{LoS} , is independently generated by Clarke's model as $h_{n,LoS} \sim \mathcal{CN}(0, \frac{\Gamma_h}{1+K_h})$. Therefore, h can be represented as

$$h = \sqrt{\frac{\Gamma_h K_h}{1 + K_h}} \exp\left(j2\pi n \frac{f}{f_s}\right) a_h(\theta_h, \phi_h) + h_{n,LoS}.$$
 (5)

Likewise, h_v can be denoted as

$$\boldsymbol{h}_{v} = \sqrt{\frac{\Gamma_{h} K_{h}}{1 + K_{h}}} \exp\left(j2\pi n \frac{f}{f_{s}}\right) \boldsymbol{a}_{hv}(\theta_{hv}, \phi_{hv}) + \boldsymbol{h}_{v,n,LoS},$$
(6)

where $h_{v,n,LoS}$ represents the non-LoS component of h_v . Following the same approach, each of g and g_v can be defined in terms of LoS and non-LoS components. It is worth mentioning that P_s , P_d , P_r , P_u , and their associated channels follow the bijection function [19], that is, each position of the communication node has a unique channel vector. This property is vital for the considered CF network and is the central feature in developing a channel prediction scheme by using a data-driven approach [19].

III. DNN-BASED CHANNEL MAPPING

In this section, we discuss how we develop an artificial intelligence (AI)-driven channel mapping algorithm that captures the correlation between the channel gains of two different configurations. It is worth mentioning that such a correlation is

mathematically intractable, and we leverage DNN to approximate the correlations by exploiting data collected from the Monte Carlo simulation framework discussed in Section IV. In this section, we first discuss the input dataset preparation, and pre-processing, then explore the DNN model architecture and proposed channel mapping algorithm.

A. Dataset Preparation

A large dataset is generated by positioning APs in different locations following uniform distributions in the $D \times D$ m² geographical area. The dataset includes the 3D coordinates of APs along with channels h and h_v . For training and simulations, h, and h_v are generated via MATLAB following (5)-(6). A similar dataset is generated for different user coordinates with their channels g, and g_v .

B. Data Pre-processing

To train the DNN model properly, two pre-processing procedures are performed on the dataset. First, each complex channel gain is separated into its real and imaginary parts and then fed to the network. The data values are then rescaled using a conventional normalization approach to confine the dataset within the range [-1;1].

C. DNN Architecture

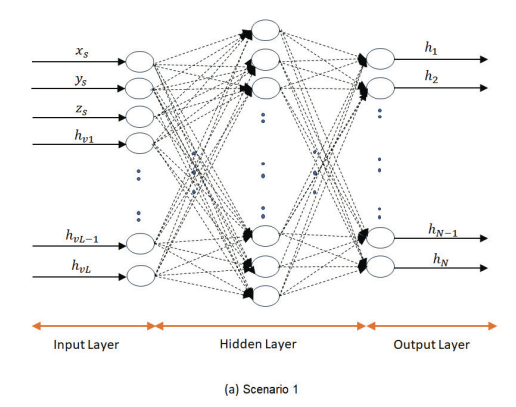
We develop a fully connected and feed-forward DNN-based channel mapping scheme. The nature of the problem requires the appropriate learning approach to be **supervised learning**. It consists of (i) an input layer \mathcal{I} , (ii) \mathcal{W} hidden layers with N_w neurons, $w \in \{1, 2, \ldots, \mathcal{W}\}$ in each layer, $N_w > 2N$, iii) an output layer \mathcal{I} , shown in Fig. 2 and 3. The hidden layers are designed optimally to predict the non-linearity of inputs. The size of N_w is selected to fit the model after numerous tests. We define α_w and β_w be the weights and bias factors of hidden layer w, respectively. With the activation function \mathcal{F} for the hidden layer w, the output from the DNN can be represented as follows:

$$\mathcal{J} = \mathcal{F}_w(\alpha_w \mathcal{F}_{w-1}(\dots \mathcal{F}_1(\alpha_1 \mathcal{I} + \beta_1) \dots) + \beta_w). \tag{7}$$

The hyperbolic tangent function $\tanh(\cdot)$ is used as the activation function in the output layer, and the leaky rectified linear unit (leaky ReLU) is deployed in the input and hidden layers as they produce effective performance in approximating the nonlinear functions. Until the model converges, the loss is reduced by the ADAptive Moment Estimation (ADAM) algorithm with a learning rate of \mathcal{L}_r . We present a four-stage algorithm for channel estimation:

1) Stage I: For a given static communication environment, there exists a deterministic mapping function ψ from every AP position P_s to their corresponding channel h [16]. The existence of position-to-channel mapping and channel-to-channel mapping is confirmed in [14]. Based on these propositions, the mapping function Ψ between two receiving antenna sets for the same transmitter was explored in Scenario 1. For Q samples, if $\{P_s\}$ is the set of all AP location P_s , and $\{h\}$, $\{h_v\}$ be the sets for h, h_v , then due to objectiveness, the position-to-channel mapping functions can be represented as follows:

$$\psi_u : \{P_{s,q}\}_{q=1}^Q \to \{\boldsymbol{h}_{v,q}\}_{q=1}^Q.$$
 (8)



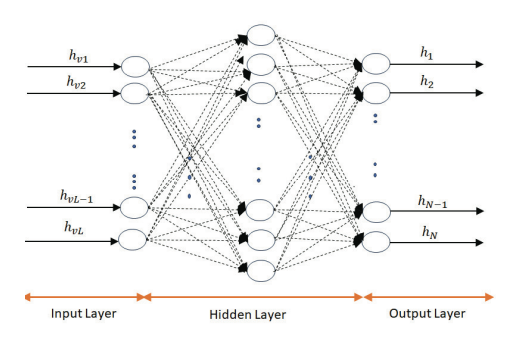


Fig. 2. DNN structure $\psi_r: \{P_{s,q}\}_{q=1}^Q \to \{\boldsymbol{h}_q\}_{q=1}^Q. \tag{9}$

Hence, the channel-to-channel mapping function can be represented as follows:

$$\Psi = \psi_u \to \psi_r : \{ \mathbf{h}_{v,q} \}_{q=1}^Q \to \{ \mathbf{h}_q \}_{q=1}^Q.$$
 (10)

In case of Scenario 1, the input layer \mathcal{I}_1 has (2L+3) neurons, $\mathcal{I}_1 \in [P_s \in \mathbb{N}^{1 \times 3}, \mathcal{RE}\{h_v \in \mathbb{C}^{L \times 1}\}, \mathcal{IM}\{h_v \in \mathbb{C}^{L \times 1}\}]$, as shown in Fig. 2. Here, $\mathcal{RE}\{\cdot\}$ and $\mathcal{IM}\{\cdot\}$ present the real and imaginary parts of a complex variable. Note that \mathcal{I}_1 is designed based on the position-to-channel mapping function ψ_u . The DNN model considered incorporates the dataset clearly, enabling it to distinguish and perform operations with better accuracy. The output layer \mathcal{J}_1 has 2N neurons, $\mathcal{J}_1 \in [\mathcal{RE}\{h \in \mathbb{C}^{N \times 1}\}, \mathcal{IM}\{h \in \mathbb{C}^{N \times 1}\}]$. The training dataset is prepared from the original dataset based on these input-output layers. The DNN model proposed for scenario 1 is then trained offline for the number of \mathcal{S} epochs.

- 2) Stage II: Following offline training, the trained model for Scenario 1 is deployed to map the channels h from h_v in real-time. At first, uplink pilot signals transmitted from AP are received by UAV. Then, channel h_v is derived by exploiting the pilot signals and associated UAV-captured channel data. Finally, channel h is mapped using the DNN.
- 3) Stage III: In Scenario 2, the channel of one AP is mapped into other neighboring APs while considering the environmental impact. In particular, the bijectivity criteria of the considered APs are exploited to realize the position-to-channel mapping function ψ_r [14]. It is worth mentioning that scenario 2 uses the outcome of Scenario 1 h. In Scenario 2, the input layer \mathcal{I}_2 has 3 neurons, $\mathcal{I}_2 \in [P_s \in \mathbb{N}^{1\times 3}]$, and the output layer \mathcal{I}_2 has 2N neurons, $\mathcal{I}_2 \in [\mathcal{RE}\{h \in$

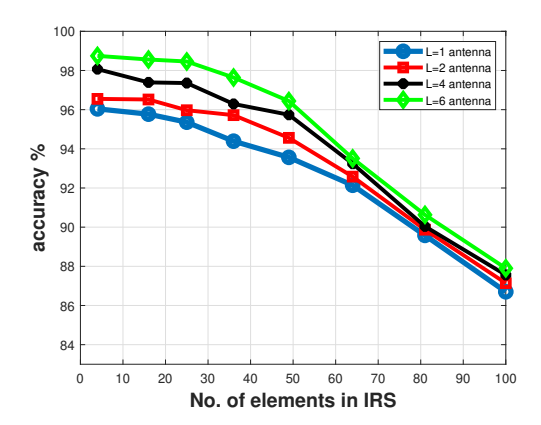


Fig. 3. Impact of the number of IRS elements on model accuracy. $\mathbb{C}^{N\times 1}$ }, $\mathcal{IM}\{h\in\mathbb{C}^{N\times 1}\}$], as shown in Fig. 2. Another training dataset is prepared from the original dataset based on these input-output layers. Finally, the proposed DNN model for Scenario 2 is trained offline for $\mathcal S$ number of epochs.

4) Stage IV: After the offline training, the trained model for Scenario 2 is deployed to map the channel h_i of AP i to the nearby channel h_j of AP j. This phenomenon is being explored to reduce the computational complexity of networkwide use cases.

D. Computational Complexity

The computational complexity of our proposed DNN model is different for the training and testing phases for both Scenarios 1 and 2. The training complexities in Stages I and III depend on forward and backward propagations [20]. The training complexity for Stage I is $\mathcal{O}(2((2L+3)N_1+2NN_{\mathcal{W}}+\sum_{w=2}^{\mathcal{W}}N_{w-1}N_w)S)$ and for Stage III is $\mathcal{O}(2(3N_1+2NN_{\mathcal{W}}+\sum_{w=2}^{\mathcal{W}}N_{w-1}N_w)S)$. However, computational complexities during real-time operations (the testing phases) in Stages II and IV depend only on forward propagation [20]. The testing complexity for Stage II is $\mathcal{O}((2L+3)N_1+2NN_{\mathcal{W}}+\sum_{w=2}^{\mathcal{W}}N_{w-1}N_w)$ and for Stage IV is $\mathcal{O}(3N_1+2NN_{\mathcal{W}}+\sum_{w=2}^{\mathcal{W}}N_{w-1}N_w)$.

IV. RESULTS AND DISCUSSIONS

In this section, we will demonstrate the performance of the proposed channel mapping scheme for CF communication systems through rigorous computer simulations.

Parameter Specifications: Throughout the experiments, we consider that 4 APs serve 2 UEs within an area of 500×500 m^2 via a UAV-mounted IRS panel. This aIRS panel is capable of hovering around adaptively to optimize the effective data throughput of the downlink and uplink. Table I lists significant

No. of elements in IRS	16 (4×4)
No. of antennas in UAV	2
Path loss factors	$\gamma_h = 3.8, \gamma_g = 2$
Ricean K-factors	$K_h = K_g = 4 \text{ dB}$
Path loss at the reference distance	$PL_0 = 30 \text{ dB}$
System Bandwidth	$f_s = 100 \text{ kHz}$
Carrier frequency	f = 2.6 GHz (S-band)
Transmit power	46 dBm
Dataset size	7000
No. of Epoch	S = 500

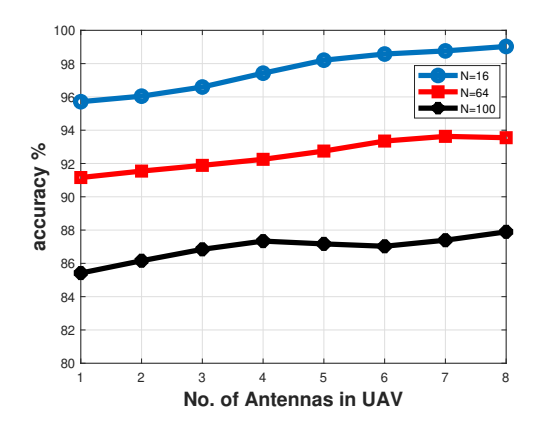


Fig. 4. Impact of number of UAV antenna on model accuracy.

parameters of the CF communication system model considered [18]. A 55 m-tall towering structure is established where the considered APs and UEs are positioned on the opposite side of the tower. The IRS-carrying UAV is hovering at a height of 61 m above the ground. We design, create, train, and evaluate the DNN model using the open-source Python libraries TensorFlow and Keras. To evaluate the performance of the proposed scheme, we calculate the normalized mean square error (NMSE) for a total number of realizations $\mathcal N$ as follows:

NMSE =
$$\frac{1}{N} \sum_{i=1}^{N} \frac{|h_i - \hat{h}_i|^2}{|h_i|^2}$$
, (11)

where h_i and \hat{h}_i denote the actual and predicted channel, respectively, for realization i. Throughout the simulations, we consider 7000 independent channel realizations and 500 epochs to train the DNN. The trained inference models are evaluated on $\mathcal{N}=100000$ realizations of channel gains to evaluate NMSE for Scenarios 1 and 2. However, the number of hidden layers and the number of neurons in each hidden layer have been set by trial and error to maximize the performance of the DNN considered. The accuracy of the model is formulated in Keras as:

$$Accuracy = \frac{1 - NMSE}{N} \times 100\%$$
 (12)

Channel Mapping for Scenario 1: In Fig. 3, we demonstrate the performance of the proposed channel mapping scheme for Scenario 1. In particular, we evaluate the accuracy of the mapped channel as a function of the number of PREs (N)for different numbers of UAV antennas $(L = \{1, 2, 4, 6\})$. We observe that for a given L, the prediction accuracy decreases with N as increasing the number of unknown elements from a fixed number of known elements without modifying the DNN design and training decreases the performance. It is worth noting that accuracy decreases significantly beyond N = 60. The prediction of a large number of unknown channels from $L \leq 6$ known channels is cumbersome due to weaker correlations between channel gains. These findings will assist system designers in determining the optimal PREto-UAV antenna ratio to implement the proposed channel mapping algorithm.

Fig. 4 compares the performance of the proposed channel mapping scheme for Scenario 1 as a function of L for N =

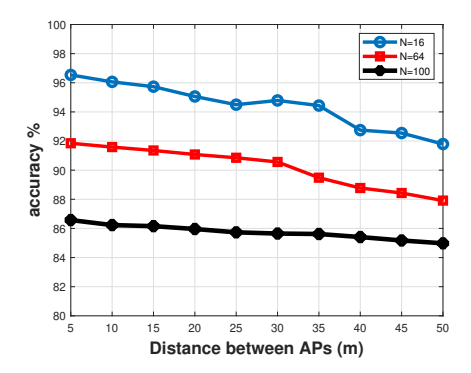


Fig. 5. Impact of inter-AP distance on model accuracy.

{16, 64, 100}. It is evident that the accuracy of the proposed scheme for predicting the channel increases with L for a given N. Increasing the number of UAV antennas and leveraging all of them to predict the channel improves the performance of channel mapping.

Channel Mapping for Scenario 2: Figs. 5 and 6 show the performance of the proposed channel mapping scheme for Scenario 2. Since the placement of APs follows a random distribution, we present the performance of the proposed scheme as functions of the mean distances between a pair of APs and a pair of AP-aIRS nodes in Figs 5 and 6, respectively.

In Fig. 5, we set a sub-region within the geographical area considered and predict the unknown channels of the AP-aIRS links from the known channels of the AP-aIRS links. We observed that the accuracy of channel prediction decreases with increasing mean distances of inter-APs. It is worth mentioning that increasing the distances among the APs decreases the spatial correlations of the underlying channels. Therefore, the proposed scheme shows degraded performance in predicting channels when the distances are larger between a pair of APs.

In Fig. 6, we present the NMSE performance of the proposed channel mapping scheme as a function of the distance between the AP and the IRS for Scenario 2. We considered three different use cases based on the number of passive reflecting elements. We observe that as the distance between the access point and the IRS increases, the NMSE also increases for all the use cases considered. However, with a larger number of passive reflecting elements, the NMSE performance improves significantly as N increases. In contrast, when the number of passive reflecting elements is small, the NMSE remains relatively stable even at greater distances.

V. CONCLUSIONS AND FUTURE WORKS

This paper proposes a DNN-based channel mapping network for the CF-MMIMO system, combining aerial-to-ground (A2G) and ground-to-aerial (G2A) communications. Based on simulation findings, the proposed model achieves its target in terms of prediction accuracy. Furthermore, we have considered different channel environments for uplink and downlink, and the proposed model excels in both environments. In this paper, users and the UAV are assumed to be in fixed positions. Future research will examine the Doppler effect, considering mobile users and mobile UAVs.

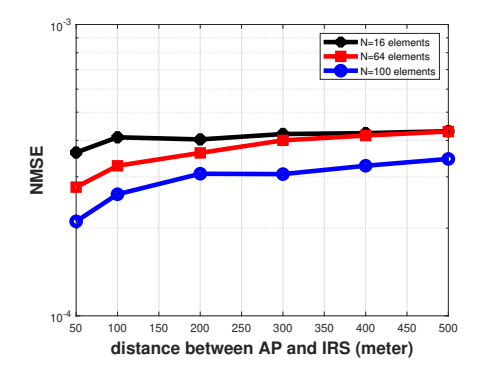


Fig. 6. Impact of AP-IRS distance on the channel.

REFERENCES

- [1] Y. J. B. L. J.Zhang, S.Chen, "Cell-free massive mimo: A new next-generation paradigm," *IEEE Access*, vol. 7, p. 99 878–99 888, 2019.
- E. Ö.T. Demir and L.Sanguinetti, "Foundations of user-centric Cell-Free Massive MIMO," *Foundations and Trends in Signal Processing*, vol. 14, no. 3-4, pp. 1994–1998, 2021.
 [3] E. B. et al., "Wireless communications through reconfigurable intelligent
- surfaces," IEEE Access, vol. 7, pp. 116753–116773, 2019.
 [4] B. Z. C. Y. Q. Wu, S. Zhang and R. Zhang, "Intelligent reflecting
- surface-aided wireless communications: A tutorial," *IEEE Transaction Communications*, vol. 69, no. 5, pp. 3313–3351, May 2021.

 [5] B. Z. C. You and R. Zhang, "Intelligent reflecting surface with discrete phase shifts: Channel estimation and passive beamforming," *IEEE*
- International Conference on Communications (ICC), p. 1–6, 2020.
 [6] W. M. C. You, B. Zheng and R. Zhang, "How to deploy intelligent reflecting surfaces in wireless network: Bs-side user-side or both sides Journal of Communications and Information Networks, vol. 7, pp. 1-10,
- [7] Y. Z. C. You, Z. Kang and R. Zhang, "Enabling smart reflection in integrated air-ground wireless network: IRS meets UAV," *IEEE Wireless*
- Commun. Mag, vol. 28, no. 6, p. 138–144, Dec. 2021. S. J. H. Lu, Y. Zeng and R. Zhang, "Aerial intelligent reflecting surface: Joint placement and passive beamforming design with 3D beam flattening," *IEEE Transactions on Wireless Communications*, vol. 20, no. 7, p. 4128–4143, Jul. 2021.

 [9] B. M. L. A. C. Pogaku, D. Do and N. D. Nguyen, "UAV-assisted DIS for future visibles are presented by the formula of the formula of the communications and the communications are communications.
- RIS for future wireless communications: A survey on optimization and performance analysis," *IEEE Access*, vol. 10, pp. 16320–16336, 2022.
- [10] M. et al., "UAV-aided aerial reconfigurable intelligent surface communications with massive mimo system," *IEEE Transactions on Cognitive* Communications and Networking, vol. 8, no. 4, pp. 1828–1838, 2022. C. Q. P.J. Zhang and P.Lu, "Channel estimation for reconfigurable intel-
- ligent surface aided Massive MIMO system," IEEE 21st International Workshop on Signal Processing Advances in Wireless Communications (SPAWC), p. 1–5, 2020. [12] Z. Y. X. Chen, J. Shi and L. Wu, "Low-complexity channel estima-
- tion for intelligent reflecting surface-enhanced massive MIMO, Wireless Communications Letters, vol. 10, no. 5, p. 996-1000, 2021.
- A. M. Elbir and S. Coleri, "Federated learning for channel estimation in conventional and IRS-assisted massive MIMO," IEEE Transactions
- on Wireless Communications, 2021.
 [14] M. Alrabeiah and A. Alkhateeb, "Deep learning for TDD and FDD Massive MIMO: Mapping channels in space and frequency," Proc. 53rd
- Asilomar Conf. Signals, Syst. Comput, p. 1465–1470, 2019.

 [15] F. G. Y. Yang and G. Y. Li, "Deep learning-based downlink channel prediction for FDD Massive MIMO systems," *IEEE Wireless Communications Letters*, vol. 23, no. 11, pp. 1994–1998, Nov. 2019.
- [16] P. K. A. M. Elbir, A. Papazafeiropoulos and S. Chatzinotas, "Deep channel learning for large intelligent surfaces aided mm-wave massive mimo systems," *IEEE Wireless Communications Letters*, vol. 9, no. 9, pp. 1447–1451, Sep. 2020.

 [17] D. B. Xiang and J.Wu, "Deep learning-based downlink channel estimation for FDD Massive MIMO systems," *IEEE Wireless Communications Letters*, vol. 12, no. 4, pp. 699–702, Apr. 2023.

 [18] C. X. et al., "Channel estimation for reconfigurable intelligent surface contents," *IEEE Transactions Letters*, vol. 75, June 1619, 2019.
- assisted high-mobility wireless systems," IEEE Trans. Veh. Technology, vol. 72, no. 1, pp. 718-734, Jan. 2023.
- "Bijection function," https://www.whitman.edu/mathematics/higher_ math_online/section04.06.html.
- I. Ahmed, M. Hasan, A. Rubaai, K. Hasan, C. Pu, and J. Reed, "Deep learning assisted channel estimation for cell-free distributed mimo networks," 2023 19th International Conference on Wireless and Mobile Computing, Networking and Communications (WiMob), pp. 344-349, $202\hat{3}$.